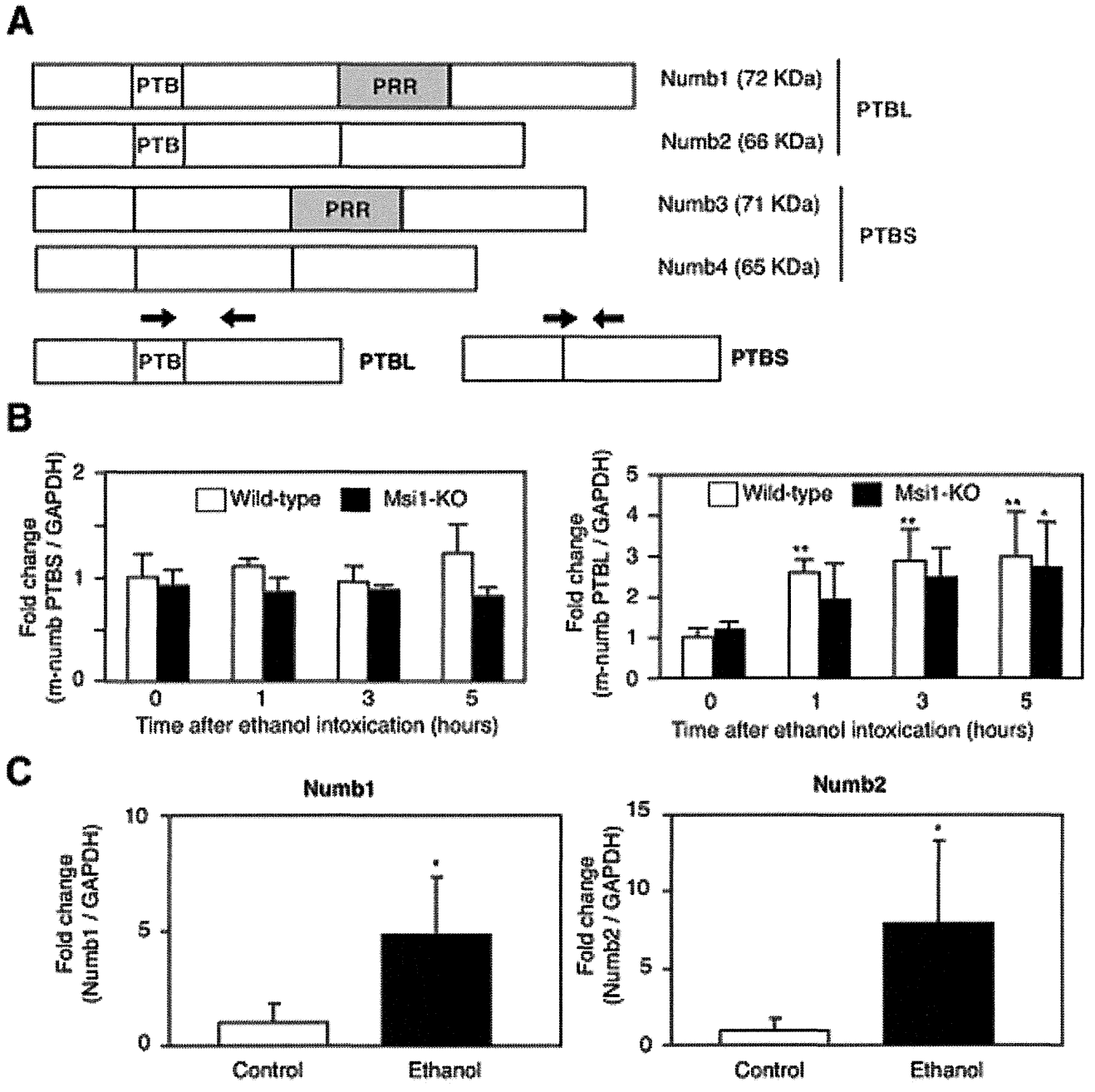

Figure 5. Expression levels of the m-Numb splicing variants in the stomach. (A) Schematic representation of the *m-Numb* gene and the primer designed for m-Numb *mRNA* amplification. (B) Expression of the PTBS- and PTBL-types of *m-Numb mRNA* in the stomach of ethanol-administered wild-type (white bars) and Msi1-KO (black bars) mice. Absolute ethanol was administered to both groups of mice and the mRNA expression of each of the splicing variants of *m-Numb* was analyzed by real-time PCR using SYBR Green. The expression levels were expressed as fold-change relative to the expression in the wild-type animals at 0 h. GAPDH was used as internal standard. (C) Semi-quantitative PCR was performed to confirm the expression of the complete PTBL-type of *m-Numb mRNA*, which was induced after gastric damage (at 5 h after ethanol administration). The primers used were the PTBL forward primer, and PRRS and PRRL reverse primers. *GAPDH* was used as the internal standard. The intensity of each band was analyzed, and the results are shown as fold-change relative to the expression in wild-type mice. *$P<0.05$ compared to Msi1-KO mice at 0 h, **$P<0.01$ compared to wild-type mice at 0 h.
doi:10.1371/journal.pone.0053540.g005

was significantly decreased in Msi1-KO mice as compared to that in wild-type mice. In addition, antioxidant factor Mt2 expression tended to be lower in Msi1-KO mice than that in the wild-type mice. The expression of PSCA and Mt2 mRNA expression was significantly induced by the overexpression of Numb1 in mouse gastric cell line, MGE507 cells (Figure 6B) as compared to that in the LacZ control (n = 4 each). Mt2 expression was also induced by Numb2 overexpression (Figure 6B). In such a gastric cells, a significant increase of the proliferative activity in PRR containing Numb1-enhanced cells was observed as compared to that in LacZ control cells ($P<0.001$; Figure 6C). In contrast, no induction of the cell proliferation activity was observed following PRR not-

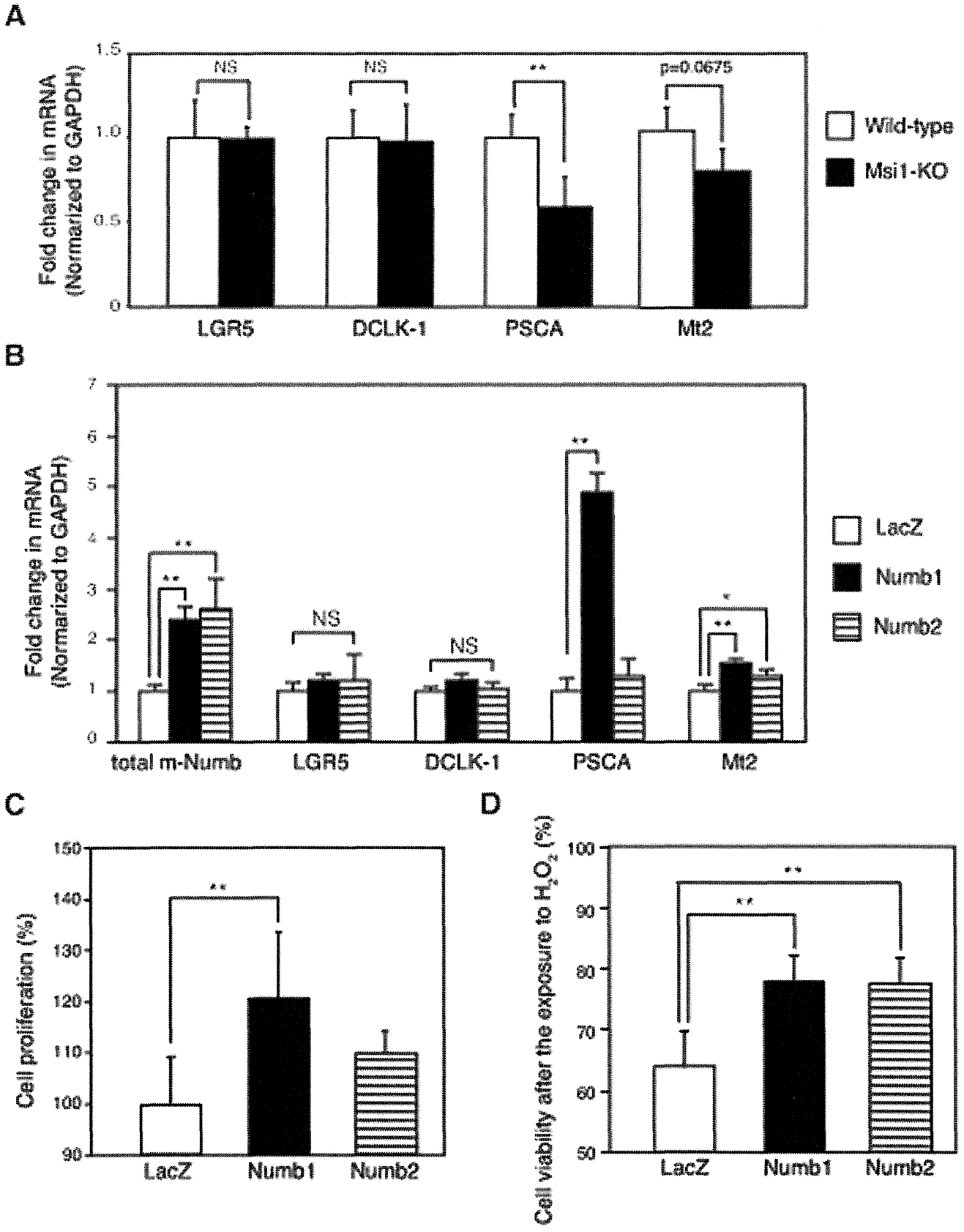

Figure 6. m-Numb-induced expression of regeneration-related genes. (A) Expression of *LGR5*, *DCLK1*, *PSCA*, and *Mt2* mRNA in the stomachs of sham-treated wild-type (white bars) and Msi1-KO (black bars) mice. $^{**}P<0.01$ compared to wild-type mice. (B) mRNA expression of total *m-numb*, *LGR5*, *DCLK1*, *PSCA*, and *Mt2* in LacZ-, Numb1-, and Numb2-overexpressing MGE507 cells. $^{*}P<0.05$, $^{**}P<0.01$ compared to LacZ-overexpressing cells.

(C) Cell proliferation assay in LacZ-, Numb1-, and Numb2-overexpressing MGE507 cells. **$P<0.01$ compared to LacZ-overexpressing cells. (D) H_2O_2-induced changes in cell viability in LacZ-, Numb1-, and Numb2-overexpressing MGE507 cells. **$P<0.01$ compared to LacZ-overexpressing cells.
doi:10.1371/journal.pone.0053540.g006

containing Numb2 enhancing under the same conditions (Figure 6C). Additionally, H_2O_2-induced cell death was significantly inhibited in Numb1 and Numb2 enhancing cells compared to that in LacZ control cells (Figure 6D).

Discussion

The present study is the first to demonstrate that upregulation of m-Numb protein expression in gastric tissues after acute gastric mucosal injury is mediated, at least in part, by Msi1. Since splicing variants of the m-Numb protein are considered to be a family of stage-specific proteins with distinct regulatory roles in neural development [23], we considered it important to clarify the expression of each splicing variant of m-Numb in this study. However, the antibody used in the study recognized the C-terminal region of the m-Numb protein, so that western blotting analysis could distinguish the presence of PRR among the m-Numb variants, but not that of PTB, because of the similarity in molecular weights. For this purpose, quantitative RT-PCR was performed using specific primers for each *m-Numb* splicing variant; this revealed splicing variant-specific induction of the PTB domain-containing *m-Numb* mRNA following gastric damage, indicating that the expression of Numb1 and Numb2, which contain PTB, is induced by gastric mucosal damage. On the other hand, although *m-Numb* mRNA was transcribed at the same level in Msi1-KO mice as in wild-type mice following gastric damage, m-Numb protein expression was decreased in the former. This suggested that m-Numb protein expression after gastric damage was post-transcriptionally downregulated by Msi1 ablation. Polysome analysis confirmed this post-transcriptional *m-Numb* regulation by Msi1.

The post-transcriptional downregulation of m-Numb protein expression by canonical Msi1-Numb-Notch axis regulation [16] has been found in wild type cerebral tissue (Figure 3A), glioblastoma U251MG [27], leukemia cells [14,15] and fibroblast NIH3T3 cells [11]. Therefore, we expected that m-Numb protein expression would be enhanced in Msi1-KO mice, as compared to wild-type mice. However, the expression of m-Numb protein in the stomach of these mice was unexpectedly downregulated compared to that in wild-type mice.

Now, we could not solve the problem about whether this posttranscriptional enhancement in the stomach was exceptional. Notably, a recent report indicates that Msi1 induces the translation of *Robo3* mRNA by 3′-UTR–independent regulation in a particular neuron in the cerebellum [28]. The stomach-specific enhancement of m-Numb translation by Msi1 may be due to the stomach-specific expression of other RNA-binding protein(s), which are involved in mRNA stabilization/translation or by a putative translational repressor of m-Numb. The molecular mechanism underlying stomach-specific regulation of *m-Numb* translation remains to be elucidated.

In several variants of m-Numb, the PRRS type of m-Numb decreases the amount of nuclear Notch than the PRRL type of m-Numb, and it inhibits cell proliferation and promotes differentiation [29]. This regulation system is identified as the canonical Numb-Notch axis. On the other hand, the PRRL type of Numb promotes cell proliferation, possibly through the noncanonical Numb-Notch axis [22]. In addition, it is reported that the PTBL type of m-Numb does not induce Notch activation [30]. In this study, we showed the decreased expression of the PTBL-PRRL (Numb1) and PTBL-PRRS (Numb2) types of m-Numb in the gastric mucosa of Msi1-KO mice with delayed regeneration, indicating that the canonical Msi1-Numb-Notch axis is not suitable for gastric tissue.

Msi1 is reported to bind to the 3′-UTR of targeted RNA, and it binds to polyA-binding protein (PABP) [31]. The interaction between Msi1 and PABP inhibits initiation of translation by competing with translation-initiation factor eIF4G for PABP [31]. Therefore, the tissue-specific variation of the *m-Numb* UTR sequence may be important for this regulation. In order to identify specific features in *m-Numb* mRNA in stomach tissues, we analyzed the structures of *m-Numb* mRNA expressed in the stomach (Methods S1). 3′-RACE yielded only the full-length 3′-UTR sequence of the *m-Numb* mRNA, which corresponds to the reference sequence (positions 2276–3644 in accession NM_001005743.1) and contains Msi1 binding site. On the other hand, 5′-RACE analysis revealed the existence of gastric-specific ΔEx2-type variants, which lack exon 2, in the 5′-UTR sequence of the *m-Numb* mRNA (Figure S6 and Result S1). Thus, it is possible that the competing reaction is attenuated in mRNAs with a ΔEx2-type 5′-UTR via conformational change, resulting in translational activation of *m-Numb*.

The present model of acute gastric injury showed that the expression of the PTB domain-containing m-Numb protein was upregulated in the damaged gastric tissues of wild-type mice, especially at the site of origin of regeneration. Furthermore, Msi1-KO mice showed weak expression of m-Numb and delayed gastric regeneration after the mucosal injury. Since the expression of the other major target gene of Msi1, i.e., *p21*, showed no change following acute gastric damage, inducible m-Numb expression may be a key event in the regulation of gastric regeneration by Msi1. Numb1, one of the two m-Numb variants upregulated after gastric damage, has the ability to induce cell proliferation, which is important for tissue regeneration. Although PRR of Numb1 functions as SH3-binding domain and induces cell proliferation [22], the proliferation mechanism has been unclear. In this connection, we demonstrated the induction of PSCA expression and cell proliferation by Numb1enhancement in gastric cells. PSCA promotes cell proliferation through the regulation of cell cycle in prostate cell [32], suggesting that Numb1 may promote gastric cell proliferation by PSCA induction. The PSCA induction may be due to the interaction between Numb1 and transcriptional factor, which has SH3 domain. Furthermore, the PSCA is also involved in cell renewal [33] and is expressed in the isthmus of human gastric mucosa, which may contain differentiating progenitor cells [26]. The C allele of rs2294008 in *PSCA*, which results in altered subcellular localization and stability of the protein, is reported to be associated with increased risk of ulceration in metaplasia consisting of gastric-type mucous secreting cells [34]. Thus, Numb1 may promote gastric regeneration through the regulation of progenitor cell function like cell proliferation by the induction of PSCA.

In addition, PTBL type of m-Numb, Numb1 and Numb2, induced mRNA expression of *Mt2*, which has anti-oxidant activity. Metallothionein transcription is mainly regulated by metal-regulatory transcription factor 1 (MTF-1), which binds to DNA sequence motifs of metallothionein, known as metal response elements (MREs) via the zinc finger domain of MTF-1 [35,36,37]. So induced Mt2 mRNA expression by PTBL type of m-Numb may be due to the regulation of MTF-1-MREs binding activity or

the direct binding of ligand of Numb, LNX, which interacts to Numb PTB [38,39] and contains zinc fingers. Mt2-induced gastric cells by m-Numb enhancement were resistant to H_2O_2-induced oxidative stress. Mt2 is important for the protection and regeneration of gastric lesions [40,41], indicating that the process of gastric regeneration mediated by m-Numb is related to the antioxidant activity of Mt2, in addition to the enhancement of progenitor cell function due to the PSCA expression (Figure 7).

We used the acute gastric injury model with ethanol administration. In this model, the basal lamina is intact, and restitution can resurface the epithelium within 2–5 h [1,2,3], indicating that this is a suitable model to estimate the initial processes of gastric regeneration. In this study, we also observed severe gastric erosion 1 h after ethanol administration in both wild-type and Msi1-KO mice. Thus, Msi1 is a key regulatory factor for the initial regeneration of gastric mucosa. Furthermore, we need to investigate the whole regeneration process in Msi1-KO mice by using other models like the acetic acid model.

In conclusion, our findings, for the first time, provide direct evidence linking Msi1 to gastric regeneration using Msi1-KO mice. Furthermore, our results suggest that Msi1 post-transcriptionally enhances PTB domain-containing m-Numb protein expression after acute gastric mucosal injury. The enhancing m-Numb expression may be a novel and specific target for the gastric ulcer treatment and epithelial regeneration.

Materials and Methods

Ethics Statement

All experiments and procedures in our study were conducted with the approval of the Keio University Animal Research Committee (No. 08079). All the animal experiments were conducted according to the Guidelines for the Care and Use of Laboratory Animals of the Keio University School of Medicine, and every effort was made to minimize suffering of the animals. Mice were specific pathogen-free, and fed with complete pelleted chow and tap water *ad libitum* in a room with controlled light (12 h light, 12 h darkness).

Animals

For generating the acute gastric mucosal injury model, ICR/CD1 background male Musashi-1-null mice [42] (10 to 20 weeks old) were used, with age-matched male wild-type ICR/CD1 littermate mice as controls. The mice were anesthetized with diethyl ether, and sacrificed after food deprivation for 18 h, after which the gastric tissues were dissected.

Rapid Gastric Mucosal Injury

Absolute ethanol (8 ml/kg) was administered to the mice by gavage after 18 h of food deprivation. The stomachs were resected 1, 3, or 5 h after ethanol administration and opened along the greater curvature.

Immunohistochemical Staining

The antibodies used for the immunohistochemical staining of the gastric mucosal paraffin sections of the mice were as follows: mouse monoclonal anti-H^+, K^+-ATPase alpha-subunit antibody (clone 1H9, 1:300, Research Diagnostics Inc., Flanders, NJ, USA) against parietal cells, rabbit anti-mouse pepsinogen antibody (mPep) against zymogenic cells, and mouse monoclonal anti-Muc6 antibody (HIK1083, 1:30, Kanto Chemical, Tokyo, Japan), originally raised against rat gastric mucin, to detect mucin-6 (Muc6) in the mammalian gastric fundic mucous neck cells and pyloric gland cells. Muc6 is identical to the class III mucin detected by paradoxical concanavalin A staining.

After opening the stomachs along the greater curvature, the specimens were fixed overnight in 10% neutralized buffered formalin and processed by the routine method for paraffin

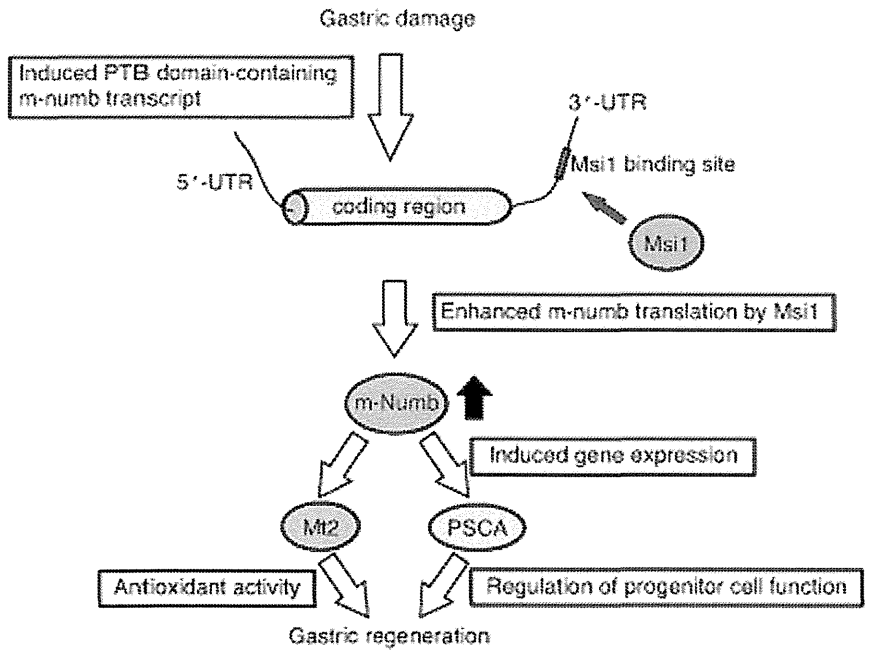

Figure 7. Schematic representation of Msi1-dependent gastric regeneration. After gastric damage, PTB domain-containing *m-numb* transcript is induced. Msi1 enhances the *m-numb* translation. The translated m-Numb protein induces the expression of regeneration-related genes such as *PSCA* and *Mt2*, resulting in gastric regeneration.
doi:10.1371/journal.pone.0053540.g007

embedding. The sections were then stained with hematoxylin and eosin (H&E) using the standard technique.

For labeling with anti-mouse pepsinogen antibody, the sections were incubated in a citrate buffer solution (10 mM, pH 6.0) at 121°C for 15 min. For labeling with anti-H^+, K^+-ATPase, and anti-Muc6 antibodies, the sections were digested with proteinase K solution (Dako, Tokyo, Japan) for 4 min at room temperature. After antigen retrieval, endogenous peroxidase activity was quenched by treatment with 0.3% hydrogen peroxide in methanol for 15 min, and the sections were then treated with a blocking reagent (Protein Block Serum-Free, Dako), followed by incubation overnight with the primary antibodies at 4°C. Then, the sections were incubated with horseradish peroxidase (HRP)-labeled anti-rabbit IgG or HRP-labeled anti-mouse IgG (Histofine, Simple stain MAX-PO goat/rabbit/mouse; Nichirei, Tokyo, Japan) for 30 min at room temperature. This was followed by color development with a solution of 3, 3′-diaminobenzidine tetrahydrochloride. For single immunohistochemical staining, counterstaining was performed with Gill's hematoxylin. The stained sections were examined using a light microscope equipped with a 3CCD digital camera (C7780; Hamamatsu Photonics, Hamamatsu, Japan).

Evaluation of Gastric Epithelial Cell Degeneration

The area of gastric erosion in the gastric fundus, identified by positive staining of the parietal cells with the anti-H^+, K^+-ATPase alpha-subunit antibody, was estimated in sections stained with H&E. The area of gastric epithelial cell degeneration was expressed as a percentage of the total area.

Reverse Transcription-polymerase Chain Reaction

Total RNA was isolated from the stomachs of mice, using the RNeasy Mini Kit (Qiagen, Germantown, MD, USA). First-strand cDNA synthesis was performed using a PrimeScript™ RT Reagent Kit (Takara Bio, Shiga, Japan).

Real-time PCR amplification was performed using a SYBR Premix Ex Taq Perfect Real Time kit (Takara Bio), in a Thermal Cycler Dice Real Time System (Takara Bio). The specific primers for amplifying mouse total *m-numb*, as well as the individual isoforms of *m-numb*, *LGR5*, *DCLK1*, *PSCA*, *Mt2*, *and glyceraldehyde-3-phosphate (GAPDH)* mRNAs (the latter as internal control) are listed in Table 1. The primers for the total *m-numb* mRNA amplified all the *m-numb* splicing variants. The 2-step PCR program was as follows: 95°C for 2 min followed by 40 cycles, each consisting of 95°C for 5 s and 60°C for 30 s.

For semi-quantitative PCR, each cDNA was amplified using KOD plus Taq (Toyobo, Osaka, Japan). The primers used to detect the Numb1 and Numb2 mRNAs were PTBL forward, PRRL reverse (5′-ATGGCTGCAATTTCCTTGTT-3′), and PRRS reverse (5′-ACCCCACTCAGTCCCTTGTA-3′). The primers for GAPDH were the same as those used for the real-time PCR. The annealing temperature was 57°C for GAPDH and 60°C for Numb1 and Numb2.

Western Blotting

The primary antibodies used for western blotting were as follows: goat polyclonal anti-m-Numb (1:2000, Abcam, Cambridge, UK), which recognized the 14 C-terminal residues of m-Numb, rabbit polyclonal anti-p21 (1:200, Santa Cruz Biotechnology, Santa Cruz, CA, USA), rat monoclonal anti-Msi1 clone 14H1 [43] (1:1,000), monoclonal anti-Msi2 (1:1,000, GeneTex, Irvine, CA, USA), and mouse monoclonal anti-β-actin clone AC-15 (1:10,000, Sigma-Aldrich, St. Louis, MO, USA), which recognized β-actin used as the internal standard.

Each tissue was lysed in ice-cold RIPA lysis buffer containing a protease inhibitor cocktail (Sigma-Aldrich). The resulting protein lysate was boiled in LDS sample buffer (Invitrogen) and separated by 4–12% NuPAGE Bis-Tris gel (Invitrogen, Carlsbad, CA, USA) electrophoresis using MOPS running buffer (Invitrogen). After electrophoresis, gels were blotted onto polyvinylidene difluoride membranes in NuPAGE Transfer buffer (Invitrogen). Membranes were blocked with a solution containing BlockAce (Dainippon Sumitomo Pharma Co., Osaka, Japan) for 1 h and incubated overnight with the primary antibody at 4°C, followed by incubation with HRP-conjugated secondary antibody for 1 h at room temperature. Thereafter, a chemiluminescence solution (GE Healthcare, Buckinghamshire, UK) was applied, and images were acquired using a FUJI LAS4000mini (GE Healthcare).

Polysome Gradient Fractionation From Gastric Tissues

Preparation of gastric tissue for polysome analysis was performed essentially according to previously described methods [44]. A 20-mg piece of solid tissue was lysed in 1 ml of lysis buffer (10 mM Tris-HCl at pH 8.0, 150 mM NaCl, 5 mM $MgCl_2$, 1% Nonidet-P40, 40 mM dithiothreitol, 1000 U/ml RNAase inhibitor (Toyobo), 40 mM vanadyl ribosyl complex (New England Bio Labs, Ipswich, MA, USA) supplemented with 1% deoxycholic acid sodium salt monohydrate (Nacalai Tesque, Inc., Kyoto, Japan). After the cells were lysed by pipetting, the nuclei were removed by centrifugation (12,000 × *g* for 10 s at 4°C). The supernatant was supplemented with 500 µL of extraction buffer (0.2 M Tris-HCl at pH 7.5, 0.3 M NaCl), 150 µg/ml cycloheximide, 650 µg/ml heparin, and 10 mM phenylmethylsulfonyl fluoride, and then

Table 1. Primer sequences for quantitative RT-PCR.

Target gene	Forward primer (5′- 3′)	Reverse primer (5′- 3′)
total *m-numb*	ACTACGGCAAAGCTTCAGGA	ACGTGGCCGAGGTACTTAAC
m-numb PTB domain containing form (PTBL)	GAAAGGAAGTTCTTCAAAGG	CCACAACTCTGAGCCCATC
m-numb PTB domain-non-containing form (PTBS)	GATTGAAAGCTACGGGAAAG	AAGTTCCTATCTGGGGCACA
LGR5	CCAAGGGAGCGTTCACGGGC	CACGTAGCTGATGTGGTTGG
DCLK-1	CAGCCTGGACCAGCTGGTGG	TGACCAGTTGGGGTTCACAT
PSCA	CCGTCTTCTTTCTCCTGCTG	CGCGATGTAAAGCAACTGTG
Mt2	TCCACTCGCCATGGACCCCA	CAGCCCTGGGAGCACTTCGC
GAPDH	TGTGTCCGTCGTGGATCTGA	TTGCTGTTGAAGTCGCAGGAG

doi:10.1371/journal.pone.0053540.t001

centrifuged (12,000 × *g* for 5 min at 4°C) to remove mitochondria and membranous debris.

The supernatant was then layered onto a 36-ml linear sucrose gradient (15–40% sucrose [w/v], supplemented with 10 mM Tris-HCl at pH 7.5, 140 mM NaCl, 1.5 mM $MgCl_2$, 10 mM dithiothreitol, 100 μg/ml cycloheximide, 0.5 mg/ml heparin) and centrifuged in a Beckman SW28 rotor for 205 min at 28,000 rpm at 4°C, with the brake off. Fractions (2 ml) were collected by adding 40% ethanol and 0.6 M guanidine (final concentration). Then, 100 μg of proteinase K in 1% SDS and 10 mM EDTA were added, and digestion was allowed to continue for 30 min at 37°C.

Total RNA from each fraction was recovered by extraction with an equal volume of phenol-chloroform-isoamyl alcohol, followed by ethanol precipitation. The quantity of *m-numb mRNA* in each fraction was determined using the total m-Numb primers and One-Step SYBR® PrimeScript™ PLUS RT-PCR kit (Takara Bio). These data are presented as percentage of the total amount of RNA in each fraction.

Preparation of Lentivirus Particles

Lentiviral mouse Numb1 and Numb2 expression vectors were constructed by inserting the corresponding cDNA sequence into the CSII-CMV-MCS-IRES2-Bsd lentiviral expression vector (kindly provided by H. Miyoshi, RIKEN). A shRNA-containing pGIPZ lentiviral vector was acquired from Open Biosystems (Huntsville, AL, USA). The respective lentiviral vectors were co-transfected with lentiviral packaging vectors into HEK-293T cells to produce mouse Numb1, Numb2, and shRNA-carrying lentiviral particles. Culture supernatants were collected 48 h after incubation and filtered through 0.45-μM membranes to generate cell-free virus.

Knockdown Expression using shRNA-containing Lentivirus Particles

Human gastric cell line N87 cells were obtained from American Type Culture Collection. The cells were transduced by the shRNA-carrying lentiviral particles using Viromag R/L beads (OZbiosciences, Marseille, France) at multiplicities of infection 100, and these cells were cultured for a week in the presence of puromycin (10 μg/ml). A non-silencing shRNA control with no homology to known mammalian genes was used as negative control for the knockdown experiment.

Over Expression of m-numb

An overexpression study of m-Numb was carried out in the mouse gastric cell line MGE507, which was established from transgenic mice harboring temperature-sensitive simian virus 40 large T antigen [45]. The cells expressed mRNAs of muc5ac, the α-subunit of the H^+, K^+-ATPase, and pepsinogen F [45]. The cells were transduced by the mouse Numb1 and Numb2-carrying lentiviral particles using Viromag R/L beads at multiplicities of infection 100, and these cells were cultured for a week in the presence of blasticidin (5 μg/ml). A LacZ gene- carrying lentiviral particle was used as a control.

Cell Viability Assay

To evaluate the rate of cell proliferation, MGE507 cells were plated at a density of 5×10^3 cells/well on 96-well plate in Dulbecco's modified Eagle medium/Ham's F-12 (DMEM/F-12: Sigma-Aldrich) supplemented with 1% FBS. After 24 hour's incubation at 37°C, Cell Count Reagent SF (Nacalai Tesque) were added to the culture medium at 10% of final concentration and further incubated for 3 h at the end of the culture. The absorbance at 450 nm (reference at 650 nm) of each well was measured. In the experiments in which the cytotoxic effect of H_2O_2 was analyzed, MGE507 cells were plated at a density of 10^4 cells/well on 96-well plate in DMEM/F-12 medium supplemented with 5% FBS. After 18 h at 37°C, the cells were washed, incubated for 1 h in serum free medium. Then, they were exposed to 500 μM H_2O_2 in serum free medium and incubated for another 2 h. Finally, they were washed twice with serum free medium, 10 μl of Cell Count Reagent SF were added to 100 μl of the culture for 3 h at the end of the culture. The absorbance at 450 nm (reference at 650 nm) of each well was measured.

Statistical Analysis

All the data were expressed as mean (SD). To define statistically significant differences between the 2 groups, the data were subjected to Student's *t*-test or Welch's *t*-test. The analysis was performed using a personal computer with the DA Stats software (ver. 1.0, freeware soft, copyright® 1993, by Dr. O. Nagata), after examination of the variances of the data using the F-test.

For multiple-group comparisons, comparisons between groups were performed using one-way ANOVA, followed by multiple comparison testing using Tukey's test, with PRISM4 software for Macintosh (GraphPad Software Inc., San Diego, CA, USA).

Supporting Information

Figure S1 Schematic representation of *m-Numb* splicing variant.
(PDF)

Figure S2 Immunohistochemical analysis in the control group. Wild-type (A, C, and E) and Msi1-KO (B, D, and F) mice were administered water. Sections of the gastric mucosa from each mouse were then stained using anti-H^+, K^+-ATPase- (A and B), anti-Muc6- (C and D), and anti-pepsinogen- (E and F) antibodies. Bar = 100 μm.
(PDF)

Figure S3 m-Numb expression in the mouse gastric tissue. The stomachs of sham-treated wild-type mice were fixed in 4% paraformaldehyde, and frozen sections were prepared. Each of the sections was stained using anti-m-Numb primary antibody and Alexa-488-conjugated anti-rabbit IgG secondary antibody. Counterstaining was performed using the anti-H^+, K^+-ATPase alpha-subunit primary antibody and Alexa-568-conjugated anti-mouse IgG secondary antibody. Bars = 100 μm.
(PDF)

Figure S4 Expression of m-Numb proteinin in the various tissues of the wild-type and Msi1-KO mice. The amount of protein from the tissues loaded in each lane for western blotting was as follows; cerebrum, cerebellum and lung; 5 μg/lane, others; 30 μg/lane. Wt; w ild-type, KO; Msi1-KO.
(PDF)

Figure S5 Numb PTBS RT minus quantitative PCR assay. Amplification of Numb-PTBS variant mRNA was performed by realtime quantitative PCR using templates of RT plus or minus RNAs from sham-treated wild-type and Msi1-KO mice of stomach. cDNA; RT plus templates, RT(-); RT minus templates.
(PDF)

Figure S6 Variation of m-Numb 5′-UTR. (A) Schematic representation of human Numb1 reference sequence (accession NM_001005743.1) (B) Ratio of each *m-Numb* 5′-UTR variant.

E. coli transformed with the ligation product of the TA-cloning vector and RACE PCR amplicon of *m-Numb* was cultured, and the type of 5′-UTR variant in the resulting colony determined by DNA sequencing and PCR. Fifty colonies each resulting from stomach and brain constructs were sequenced.
(PDF)

Methods S1 Fluorescent immunostaining of the m-Numb protein in the mouse gastric tissues. The mouse gastric tissue specimens were fixed with 4% paraformaldehyde and frozen sections were prepared. For fluorescent immunostaining of the human gastric tissues, paraffin sections of human gastric tissue specimens were deparaffinized, rehydrated and treated with antigen retrieval solution at 90°C for 20 min (Nacalai tesque, Kyoto, Japan). The sections were then treated with a blocking reagent and incubated overnight with rabbit anti-m-Numb antibody (1:200, Abcam, Cambridge, UK) at 4°C. The sections from the mice were further incubated with mouse monoclonal anti- H^+, K^+-ATPase antibody, followed by washing with PBS and then incubation with Alexa-488-labeled anti-rabbit IgG and Alexa-568-labeled anti-mouse IgG (Molecular Probes, Eugene, OR) for 2 h at room temperature. In the human gastric tissue sections, nuclei were visualized with 4', 6-diamidino-2-phenylindole (DAPI) (Sigma-Aldrich). The prepared sections were examined under a Zeiss LSM510 laser scanning confocal microscope (Zeiss Microimaging, Thornwood, NY). ***RACE analysis:*** Rapid amplification of cDNA 3′-ends (3′-RACE) and 5′-ends (5′-RACE) experiments were performed using SMARTer^{TM} RACE cDNA Amplification Kit (Clontech, Palo Alto, CA, USA). Human normal brain and stomach RNA (Takara Bio) were used as templates. The cDNA generated by RACE was amplified by PCR using the universal primer A mix, provided by the manufacturer, and a gene-specific primer. The gene-specific primers for 3′-RACE and 5′-RACE were as follows: 3′-RACE: 5′-CAGCAGACAGGCATACAGAGGTTCCT-3′, and 5′-RACE: 5′-TCCGGTGCGAACGCCTTCTT-3′. The resulting PCR amplicon was ligated into the pMD20 TA cloning vector (Takara Bio). The ligation products were then used to transform *E. coli* DH5α competent cells. After transformation, the integrity of the inserted sequence was determined by DNA sequencing.
(DOC)

Result S1 UTR analysis. Only full-length 3′-UTR sequence of *m-Numb mRNA* was obtained by 3′-RACE in both stomach and brain; this sequence corresponded to the reference sequence (positions 2276–3644 in accession NM_001005743.1; Figure S6A). On the other hand, 5′-RACE analysis revealed splicing variants lacking exon 2 (ΔEx2) or exon 3 (ΔEx3) in the 5′-UTR sequence of *m-Numb mRNA*. Among 50 colonies of transformed *E. coli* derived from stomach or brain products of 5′-RACE, the ΔEx2 variant of the 5′-UTR was only detected in the colonies derived from the stomach (Figure S6B).
(DOC)

Acknowledgments

We thank Dr. Hiroyuki Miyoshi at RIKEN Tsukuba Institute for the CSII-CMV-MCS-IRES2-Bsd plasmids.

Author Contributions

Conceived and designed the experiments: TT HS TI HO. Performed the experiments: TT. Analyzed the data: TT HS TI SS HO. Contributed reagents/materials/analysis tools: SS YT HO. Wrote the paper: TT HS TI SS HO. Supervised the experiments and their analysis: KT HO TH.

References

1. Lacy ER, Ito S (1984) Rapid epithelial restitution of the rat gastric mucosa after ethanol injury. Lab Invest 51: 573–583.
2. Ito S, Lacy ER, Rutten MJ, Critchlow J, Silen W (1984) Rapid repair of injured gastric mucosa. Scand J Gastroenterol Suppl 101: 87–95.
3. Moore R, Carlson S, Madara JL (1989) Rapid barrier restitution in an in vitro model of intestinal epithelial injury. Lab Invest 60: 237–244.
4. Sakakibara S, Imai T, Hamaguchi K, Okabe M, Aruga J, et al. (1996) Mouse-Musashi-1, a neural RNA-binding protein highly enriched in the mammalian CNS stem cell. Dev Biol 176: 230–242.
5. Okano H, Imai T, Okabe M (2002) Musashi: a translational regulator of cell fate. J Cell Sci 115: 1355–1359.
6. Okano H, Kawahara H, Toriya M, Nakao K, Shibata S, et al. (2005) Function of RNA-binding protein Musashi-1 in stem cells. Exp Cell Res 306: 349–356.
7. Nakamura M, Okano H, Blendy JA, Montell C (1994) Musashi, a neural RNA-binding protein required for Drosophila adult external sensory organ development. Neuron 13: 67–81.
8. Okabe M, Imai T, Kurusu M, Hiromi Y, Okano H (2001) Translational repression determines a neuronal potential in Drosophila asymmetric cell division. Nature 411: 94–98.
9. Nagata H, Akiba Y, Suzuki H, Okano H, Hibi T (2006) Expression of Musashi-1 in the rat stomach and changes during mucosal injury and restitution. FEBS Lett 580: 27–33.
10. Battelli C, Nikopoulos GN, Mitchell JG, Verdi JM (2006) The RNA-binding protein Musashi-1 regulates neural development through the translational repression of p21WAF-1. Mol Cell Neurosci 31: 85–96.
11. Imai T, Tokunaga A, Yoshida T, Hashimoto M, Mikoshiba K, et al. (2001) The neural RNA-binding protein Musashi1 translationally regulates mammalian numb gene expression by interacting with its mRNA. Mol Cell Biol 21: 3888–3900.
12. Charlesworth A, Wilczynska A, Thampi P, Cox LL, MacNicol AM (2006) Musashi regulates the temporal order of mRNA translation during Xenopus oocyte maturation. Embo J 25: 2792–2801.
13. de Sousa Abreu R, Sanchez-Diaz PC, Vogel C, Burns SC, Ko D, et al. (2009) Genomic analyses of musashi1 downstream targets show a strong association with cancer-related processes. J Biol Chem 284: 12125–12135.
14. Ito T, Kwon HY, Zimdahl B, Congdon KL, Blum J, et al. (2010) Regulation of myeloid leukaemia by the cell-fate determinant Musashi. Nature 466: 765–768.
15. Kharas MG, Lengner CJ, Al-Shahrour F, Bullinger L, Ball B, et al. (2010) Musashi-2 regulates normal hematopoiesis and promotes aggressive myeloid leukemia. Nat Med 16: 903–908.
16. Nishimoto Y, Okano H (2010) New insight into cancer therapeutics: induction of differentiation by regulating the Musashi/Numb/Notch pathway. Cell Res 20: 1083–1085.
17. Matsuda Y, Wakamatsu Y, Kohyama J, Okano H, Fukuda K, et al. (2005) Notch signaling functions as a binary switch for the determination of glandular and luminal fates of endodermal epithelium during chicken stomach development. Development 132: 2783–2793.
18. Roegiers F, Jan YN (2004) Asymmetric cell division. Curr Opin Cell Biol 16: 195–205.
19. Uemura T, Shepherd S, Ackerman L, Jan LY, Jan YN (1989) numb, a gene required in determination of cell fate during sensory organ formation in Drosophila embryos. Cell 58: 349–360.
20. Zhong W, Feder JN, Jiang MM, Jan LY, Jan YN (1996) Asymmetric localization of a mammalian numb homolog during mouse cortical neurogenesis. Neuron 17: 43–53.
21. Kuo CT, Mirzadeh Z, Soriano-Navarro M, Rasin M, Wang D, et al. (2006) Postnatal deletion of Numb/Numblike reveals repair and remodeling capacity in the subventricular neurogenic niche. Cell 127: 1253–1264.
22. Verdi JM, Bashirullah A, Goldhawk DE, Kubu CJ, Jamali M, et al. (1999) Distinct human NUMB isoforms regulate differentiation vs. proliferation in the neuronal lineage. Proc Natl Acad Sci U S A 96: 10472–10476.
23. Bani-Yaghoub M, Kubu CJ, Cowling R, Rochira J, Nikopoulos GN, et al. (2007) A switch in numb isoforms is a critical step in cortical development. Dev Dyn 236: 696–705.
24. Dho SE, French MB, Woods SA, McGlade CJ (1999) Characterization of four mammalian numb protein isoforms. Identification of cytoplasmic and membrane-associated variants of the phosphotyrosine binding domain. J Biol Chem 274: 33097–33104.
25. Corallini S, Fera S, Grisanti L, Falciatori I, Muciaccia B, et al. (2006) Expression of the adaptor protein m-Numb in mouse male germ cells. Reproduction 132: 887–897.
26. Sakamoto H, Yoshimura K, Saeki N, Katai H, Shimoda T, et al. (2008) Genetic variation in PSCA is associated with susceptibility to diffuse-type gastric cancer. Nat Genet 40: 730–740.
27. Muto J, Imai T, Ogawa D, Nishimoto Y, Okada Y, et al. (2012) RNA-binding protein Musashi1 modulates glioma cell growth through the post-transcriptional

regulation of Notch and PI3 kinase/Akt signaling pathways. PLoS One 7: e33431.
28. Kuwako K, Kakumoto K, Imai T, Igarashi M, Hamakubo T, et al. (2010) Neural RNA-binding protein Musashi1 controls midline crossing of precerebellar neurons through posttranscriptional regulation of Robo3/Rig-1 expression. Neuron 67: 407–421.
29. Toriya M, Tokunaga A, Sawamoto K, Nakao K, Okano H (2006) Distinct functions of human numb isoforms revealed by misexpression in the neural stem cell lineage in the Drosophila larval brain. Dev Neurosci 28: 142–155.
30. Kyriazis GA, Belal C, Madan M, Taylor DG, Wang J, et al. (2010) Stress-induced switch in Numb isoforms enhances Notch-dependent expression of subtype-specific transient receptor potential channel. J Biol Chem 285: 6811–6825.
31. Kawahara H, Imai T, Imataka H, Tsujimoto M, Matsumoto K, et al. (2008) Neural RNA-binding protein Musashi1 inhibits translation initiation by competing with eIF4G for PABP. J Cell Biol 181: 639–653.
32. Zhao Z, Ma W, Zeng G, Qj D, Ou L, et al. (2011) Small interference RNA-mediated silencing of prostate stem cell antigen attenuates growth, reduces migration and invasion of human prostate cancer PC-3M cells. Urol Oncol.
33. Gu Z, Thomas G, Yamashiro J, Shintaku IP, Dorey F, et al. (2000) Prostate stem cell antigen (PSCA) expression increases with high gleason score, advanced stage and bone metastasis in prostate cancer. Oncogene 19: 1288–1296.
34. Tanikawa C, Urabe Y, Matsuo K, Kubo M, Takahashi A, et al. (2012) A genome-wide association study identifies two susceptibility loci for duodenal ulcer in the Japanese population. Nat Genet 44: 430–434, S431–432.
35. Westin G, Schaffner W (1988) A zinc-responsive factor interacts with a metal-regulated enhancer element (MRE) of the mouse metallothionein-I gene. Embo J 7: 3763–3770.
36. Radtke F, Heuchel R, Georgiev O, Hergersberg M, Gariglio M, et al. (1993) Cloned transcription factor MTF-1 activates the mouse metallothionein I promoter. Embo J 12: 1355–1362.
37. Heuchel R, Radtke F, Georgiev O, Stark G, Aguet M, et al. (1994) The transcription factor MTF-1 is essential for basal and heavy metal-induced metallothionein gene expression. Embo J 13: 2870–2875.
38. Dho SE, Jacob S, Wolting CD, French MB, Rohrschneider LR, et al. (1998) The mammalian numb phosphotyrosine-binding domain. Characterization of binding specificity and identification of a novel PDZ domain-containing numb binding protein, LNX. J Biol Chem 273: 9179–9187.
39. Li SC, Zwahlen C, Vincent SJ, McGlade CJ, Kay LE, et al. (1998) Structure of a Numb PTB domain-peptide complex suggests a basis for diverse binding specificity. Nat Struct Biol 5: 1075–1083.
40. Mita M, Satoh M, Shimada A, Okajima M, Azuma S, et al. (2008) Metallothionein is a crucial protective factor against Helicobacter pylori-induced gastric erosive lesions in a mouse model. Am J Physiol Gastrointest Liver Physiol 294: G877–884.
41. Tran CD, Huynh H, van den Berg M, van der Pas M, Campbell MA, et al. (2003) Helicobacter-induced gastritis in mice not expressing metallothionein-I and II. Helicobacter 8: 533–541.
42. Sakakibara S, Nakamura Y, Yoshida T, Shibata S, Koike M, et al. (2002) RNA-binding protein Musashi family: roles for CNS stem cells and a subpopulation of ependymal cells revealed by targeted disruption and antisense ablation. Proc Natl Acad Sci U S A 99: 15194–15199.
43. Kaneko Y, Sakakibara S, Imai T, Suzuki A, Nakamura Y, et al. (2000) Musashi1: an evolutionally conserved marker for CNS progenitor cells including neural stem cells. Dev Neurosci 22: 139–153.
44. del Prete MJ, Vernal R, Dolznig H, Mullner EW, Garcia-Sanz JA (2007) Isolation of polysome-bound mRNA from solid tissues amenable for RT-PCR and profiling experiments. RNA 13: 414–421.
45. Tabuchi Y, Arai Y, Shioya H, Kuribayashi R, Ishibashi K, et al. (2003) New gastric epithelial cell lines from mice transgenic for temperature-sensitive simian virus 40 large T antigen show distinct types of cell differentiation. Digestion 67: 71–81.

Neurogastroenterology & Motility

Neurogastroenterol Motil (2013) doi: 10.1111/nmo.12122

Impaired heme oxygenase-1 induction in the gastric antrum induces disruption of the interstitial cells of Cajal network in a rat model of streptozotocin-induced diabetes

S. MOGAMI,*,† H. SUZUKI,* H. TSUGAWA,* S. FUKUHARA* & T. HIBI*

*Division of Gastroenterology and Hepatology, Department of Internal Medicine, Keio University School of Medicine, Tokyo, Japan

†TSUMURA Research Laboratories, TSUMURA & Co., Ibaraki, Japan

Abstract

Background *Streptozotocin (STZ) is known to induce type I diabetes and the loss of the interstitial cells of Cajal (ICC). However, the regulation of heme oxygenase-1 (HO-1) expression, which is reported to protect ICC, has not yet been elucidated in this model. The aim of this study was to investigate the alterations of HO-1 expression and clarify the mechanism of ICC loss in the stomach using the rat model of STZ-induced diabetes.* ***Methods*** *Streptozotocin (65 mg kg^{-1}) was intraperitoneally administered to 8-week-old female Wistar rats. Cobalt protoporphyrin (CoPP), an HO-1 inducer, was administered subcutaneously once a week after the STZ injection. The expressions of HO-1 and the receptor tyrosine kinase c-Kit (a marker for ICC) proteins were investigated by western blot analysis and immunofluorescence staining.* ***Key Results*** *Expression of c-Kit, particularly in the gastric antrum, was significantly decreased at 8 weeks, not at 1 week, compared to those of the control group. Significantly increased induction of HO-1 expression, especially in the gastric corpus but not in the antrum, was observed in the STZ group at 8 weeks after the STZ injection relative to control. CoPP administration significantly up-regulated HO-1 expression in the STZ diabetic group and significantly restored the previously reduced ICC in the gastric antrum.* ***Conclusions & Inferences*** *Up-regulation of HO-1 expression in the STZ diabetic model was limited to the gastric corpus and impaired up-regulation of HO-1 expression in the gastric antrum likely induced the disruption of the ICC network.*

Keywords *diabetes, M2 macrophage, oxidative stress.*

Abbreviations: c-Kit, gene product of *c-kit* receptor tyrosine kinase; CoPP, cobalt protoporphyrin; HO-1, heme oxygenase-1; ICC-IM, intramuscular interstitial cells of Cajal; ICC-MY, myenteric interstitial cells of Cajal; ICC-SM, submucosal interstitial cells of Cajal; ICC, the interstitial cells of Cajal; NOD, non-obese diabetic; Nrf2, NF-E2-related factor 2; STZ, streptozotocin; TBA-RS, thiobarbituric acid reactive substances.

INTRODUCTION

Gastroparesis and loss of interstitial cells of Cajal (ICC) have been observed in some patients[1] and in animal models of diabetes.[2,3] ICC, which express the proto-oncogene *c-kit* receptor tyrosine kinase (gene product, c-Kit), play critical roles in gastrointestinal motility.[4–6] c-Kit is essential for ICC development and maintenance of their phenotype.[7,8] Several classes of ICC have been identified in the mammalian stomach. Myenteric ICC (ICC-MY) lie in the space between the circular and longitudinal muscles in the region around the myenteric plexus and have been identified as the source of the electrical slow waves underlying the phasic contractions of the gastric musculature.[9] Intramuscular ICC (ICC-IM) are found in the circular and longitudinal muscle layers and mediate excitatory and inhibitory inputs to the musculature from the enteric motor neurons.[10,11] Submucosal ICC (ICC-SM) are located at the submucosal border of the circular muscle in the gastric antrum.[12,13]

Increased oxidative stress associated with diabetes can lead to loss of or damage to ICC in mice.

Address for Correspondence
Hidekazu Suzuki, Division of Gastroenterology and Hepatology, Department of Internal Medicine, Keio University School of Medicine, 35 Shinanomachi, Shinjuku-ku, Tokyo 160-8582, Japan.
Tel: +81 3 5363 3914; fax: +81 3 5363 3967;
e-mail: hsuzuki@a6.keio.jp
Received: 7 September 2012
Accepted for publication: 27 February 2013

Up-regulation of the enzyme heme oxygenase-1 (HO-1) is an important cellular defence mechanism against oxidative stress.[14] HO-1 and its product, carbon monoxide, are reported to protect ICC from oxidative stress in diabetic models.[2,15] In 20% of non-obese diabetic (NOD) mice, HO-1 up-regulation was lost and resulted in the development of delayed gastric emptying and ICC loss in both gastric corpus and antrum. Failure of HO-1 up-regulation in response to oxidative stress can induce gastroparesis and the loss of ICC in the stomach.

Streptozotocin (STZ) is known to induce type I diabetes and showed delayed gastric emptying and the loss of ICC in the gastric antrum in all diabetic rats.[3] However, the regulation of HO-1 expression in the stomach has not yet been elucidated in this rat model. The aim of this study was to investigate the alterations of HO-1 expression and clarify the mechanism of ICC loss in the stomach in the rat model of STZ-induced diabetes.

MATERIALS AND METHODS

Animals

Seven-week-old female Wistar rats were purchased from Japan SLC Inc. (Shizuoka, Japan). All rats were handled according to the guidelines of the Keio University Animal Research Committee (approved protocol No. 09140) and the Experimental Animal Ethics Committee of Tsumura & Co. (approved protocol No. 09-154). All rats were used after 1 week of acclimation and were assigned to the controls, STZ group or controls, STZ group, STZ + cobalt protoporphyrin (CoPP) group.

STZ and CoPP administration

Streptozotocin (S0130, Sigma Chemical Co., St. Louis, MO, USA) was dissolved in 20 mM citrate buffer (pH 4.5) made in physiological saline immediately before administration and was intraperitoneally administered to the STZ group (65 mg kg^{-1}). Diabetes was defined as a blood glucose level of >300 mg dL^{-1}, measured at 1 week after STZ injection, using a LifeScan ONE TOUCH Ultra Blood Glucose Monitoring System (Johnson & Johnson Company, New Brunswick, NJ, USA) with blood obtained from the tail vein. In case of CoPP treatment, blood glucose levels were measured at 4 days after STZ injection, and rats with blood glucose levels of >300 mg dL^{-1} were chosen and divided into two groups: the STZ + vehicle group (STZ group) and the STZ + CoPP group. CoPP (Co654-9, Frontier Scientific Inc., Logan, UT, USA) was first dissolved in 100 mmol L^{-1} NaOH, subsequently adjusted to a pH of 7.4 with 1 mol L^{-1} HCl, and diluted in saline to a final concentration of 1 mg mL^{-1}. The stock solution was aliquoted and stored at −80 °C until use. The vehicle solution of CoPP and CoPP was subcutaneously administered to the STZ group and the STZ + CoPP group, respectively, once a week, beginning at 4 days after STZ injection. Rats were killed under ether anaesthesia or by decapitation at 1 or 8 weeks after STZ injection.

Preparation of total RNA and quantitative reverse transcription (RT) - PCR analysis

Total RNA was extracted from the stomach tissue using the RNeasy Mini kit (Qiagen, Valencia, CA, USA). RNA was converted into cDNA using the PrimeScript RT reagent kit (Takara, Ohtsu, Japan). Quantitative real-time PCR analysis was performed using Dice (Takara) with SYBR Premix Ex TaqII (Takara). The primer sequences used were as follows; *c-kit* mRNA: 5′-ATC CAG CCC CAC ACC CTG TT-3′ and 5′-TGT AGG CAA GAA CCA TCA CAA TGA-3′, *ho-1* mRNA: 5′ -AAG AGG CTA AGA CCG CCT TC-3′ and 5′ -GCA TAA ATT CCC ACT GCC AC-3′, *GAPDH* mRNA: 5′- GGC ACA GTC AAG GCT GAG AAT G -3′, 5′- ATG GTG GTG AAG ACG CCA GTA -3′. The mRNA expression levels were normalized using the glyceraldehyde 3-phosphate dehydrogenase (GAPDH) mRNA expression levels.

Western blot analysis

Liquid nitrogen-frozen specimens of the total stomach or gastric antral smooth muscle layer were homogenized in ice-cold RIPA buffer (Upstate, Temecula, CA, USA) containing a protease inhibitor cocktail (Sigma Chemical Co.), and the supernatants were used as the total proteins. The total proteins were separated by electrophoresis and probed with an anti-HO-1 antibody (1 : 1000, SPA-895, Stressgen, Ann Arbor, MI, USA) and an anti c-Kit-antibody (1 : 1000, A4502, DAKO Japan, Tokyo, Japan), followed by reprobing with an anti-β-actin antibody (1 : 20000, clone: AC-74, Sigma Chemical Co.) as the loading control. Band quantification was performed using the ImageJ program (National Institutes of Health, Bethesda, MD, USA) and shown as '% of Normal' using the results of the normal group from the same gel.

Immunofluorescence staining

For immunofluorescence staining for HO-1 or HO-1/CD206 (double staining), stomach tissue specimens were fixed in 10% neutralized formalin and embedded in paraffin. After deparaffinization and hydration, the antigens were retrieved by heating in citrate buffer (10 mmol L^{-1}, pH 6.0). Non-specific binding was blocked using Protein Block (DAKO Japan). The sections were incubated overnight at 4 °C with an anti-HO-1-antibody (1 : 400, SPA-895, Stressgen) or anti-HO-1 antibody (1 : 200, ab13248, Abcam)/anti-CD206 antibody (1 : 5000, ab64693, Abcam). Immunoreactivity was detected using Alexa Fluor 488 goat anti-rabbit IgG (Invitrogen, Carlsbad, CA, USA) or Alexa Fluor 488 goat anti-mouse IgG/Alexa Fluor 568 anti-rabbit IgG (double staining).

For immunofluorescence staining of HO-1/CD163 (double staining) or c-Kit, stomach tissue specimens were fixed with cold acetone for 30 min and embedded in Tissue-Tek OCT compound 4583 (Sakura Finetechnical Co. Ltd. Tokyo, Japan) and cut into 5-μm sections with a cryostat (CM1850, Leica, Nussloch, Germany). The sections were incubated with Protein Block (DAKO Japan) containing 0.5% Triton X-100 for 1 h at room temperature. The sections were incubated with anti-HO-1 antibody (1 : 400, SPA-895, Stressgen), a monoclonal antibody to rat CD163 (1 : 500, T-3011, BMA Biomedicals, Augst, Switzerland) and an anti c-Kit-antibody (1 : 200, A4502, DAKO Japan) overnight at 4 °C. Immunoreactivity was detected using Alexa Fluor 488 goat anti-rabbit IgG and Alexa Fluor 568 anti-mouse IgG. Immunofluorescence was examined using a Nikon Eclipse E600 microscope (Nikon Corporation, Tokyo, Japan) or a Leica TCS SP5 system (Leica) with adequate filter cubes. The areas of the

c-Kit-positive cells were quantified using the IMAGEJ program (National Institutes of Health); the ICC-SM and ICC-MY were normalized to the length of the smooth muscle layers and the ICC-IM were normalized to the area.

HO activity assay

HO-1 activity was investigated as previously described.[2] Briefly, microsome proteins of gastric corpus homogenate (500 μg) were incubated with 20 μmol L^{-1} hemin, 3 mg of liver cytosol, 0.2 U of glucose-6-phosphate dehydrogenase, 2 mmol L^{-1} glucose-6-phosphate and 0.8 mmol L^{-1} NADPH for 1 h at 37 °C in the dark. The absorbance of produced bilirubin at 464 nm was measured at 520 nm (extinction coefficient, 40 (mmol L^{-1})$^{-1}$ cm^{-1} for bilirubin). HO-1 activity was expressed as pmol of bilirubin mg protein^{-1} h^{-1}. The total protein content of the microsome was determined using a BCA™ Protein Assay kit (Pierce, Rockford, IL, USA).

Measurement of the serum thiobarbituric acid reactive substances levels

After 24-h food deprivation, whole blood samples were obtained from the right ventricle under ether anaesthesia. Blood samples were centrifuged at 4 °C, and the supernatant was stored at −80 °C until use. The serum thiobarbituric acid reactive substances (TBA-RS) levels were determined using the TBARS Assay Kit (Cayman Chemical Company, Ann Arbor, MI, USA).

Statistical analysis

All values were expressed as means ± standard deviations (SD). The statistical significance of any differences was evaluated using the Student's *t*-test. Statistical significance was set at $P < 0.05$, unless otherwise indicated.

RESULTS

Effect of STZ injection on gastric ICC

The effect of STZ-induced diabetes on gastric ICC was investigated at 1 and 8 weeks after STZ injection. *c-kit* mRNA (38.2 ± 3.88% of Normal group) and c-Kit (75.0 ± 13.7% of Normal group) expressions were significantly decreased relative to the normal group at 8 weeks but not at 1 week (Fig. 1A and B). However, immunofluorescence staining revealed that c-Kit immunoreactivity was reduced in the gastric antrum compared to the normal group, particularly in the ICC-IM (76.2 ± 12.3% of Normal group, $P = 0.06$) and ICC-SM (68.9 ± 13.9% of Normal group, $P = 0.01$), but not in the gastric corpus at 8 weeks (Fig. 1C, D).

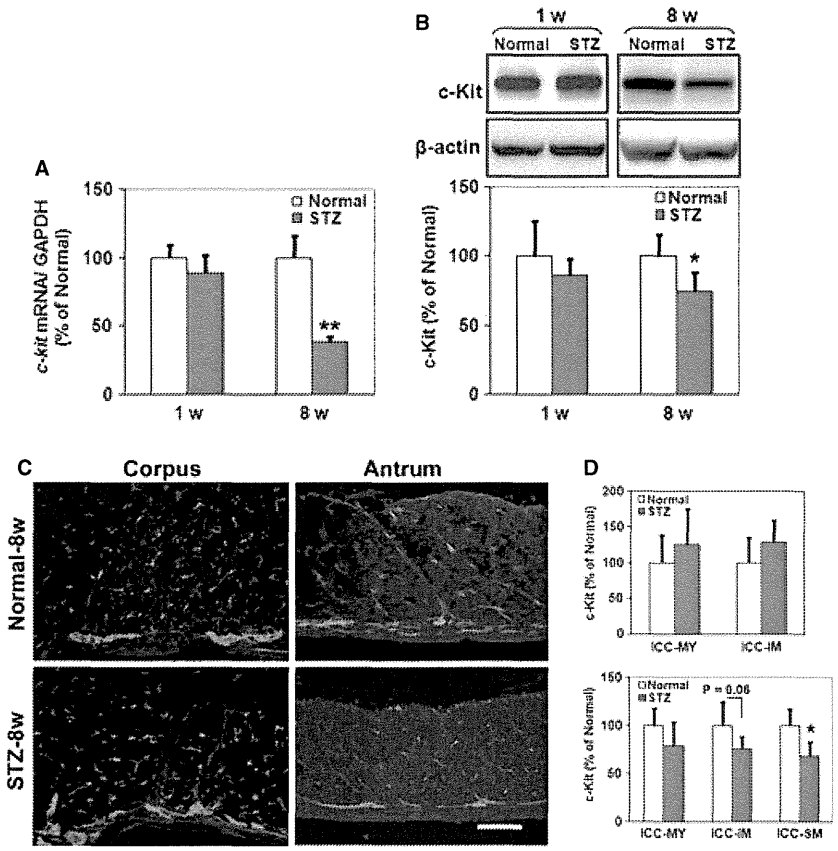

Figure 1 Expression of *c-kit* mRNA in the whole stomach (A) and expression of c-Kit protein in the smooth muscle layer of the whole stomach (B) at 1 and 8 weeks after streptozotocin (STZ) injection. A typical band from each group from the same gel is shown in the upper panel of (B). Bands were quantified and normalized using β-actin as a loading control, and the results are presented as % of Normal in the lower panel. (C) Representative image of Immunofluorescence staining for c-Kit in the smooth muscle layer in the gastric corpus (left panel) and antrum (right panel) of normal (upper panel) and STZ-induced diabetic rats (lower panel) at 8 weeks after STZ injection. Bar, 100 μm. (D) Areas of ICC-MY, ICC-IM and ICC-SM in the images of immunofluorescent staining were quantified using image analysis software. Areas of ICC in the gastric corpus are shown in the upper panel and areas of ICC in the antrum are shown in the lower panel. Normal-1w (open bar), $n = 6$; STZ-1w (filled bar), $n = 5$; normal-8w (open bar), $n = 6$; STZ-8w (filled bar), $n = 6$. Data are given as mean ± SD. $^*P < 0.05$, $^{**}P < 0.01$ compared with normal rats.

Effect of STZ injection on HO-1 expression

The effect of STZ-induced diabetes on gastric HO-1 expression was investigated at 1 and 8 weeks after STZ injection. *Ho-1* mRNA (378 ± 59.2% of Normal group) and HO-1 protein (480 ± 309% of Normal group) expressions were significantly increased relative to the normal group at 8 weeks but not at 1 week (Fig. 2A, B). HO-1 activity was also significantly increased at 8 weeks (Normal group: 15.3 ± 35.4 pmol bilirubin mg^{-1} hr^{-1}, STZ group: 70.8 ± 45.64 pmol bilirubin mg^{-1} hr^{-1}) (Fig. 2C). Serum TBA-RS levels (oxidative stress levels) were significantly increased after 1 week (Fig. 2D).

Double immunofluorescence staining for HO-1 (green) and CD163 (red, a marker for resident macrophages) was performed at 8 weeks after STZ injection. As shown in Fig. 3A and B, HO-1 was not expressed in the resident macrophages in the smooth muscle layer of normal rats. In STZ rats, HO-1 expression was induced in the resident macrophages of the gastric corpus (Fig. 3A) but not in the resident macrophages of the gastric antrum (Fig. 3B).

Double immunofluorescence staining for HO-1 (green) and CD206 (red, a marker for M2 macrophages) was also performed at 8 weeks after STZ injection. As shown in Fig. 3C and D, few CD206-positive cells were observed in the smooth muscle layer in the gastric corpus and antrum of normal rats. In STZ rats, the number of CD206-positive macrophages was markedly increased in both the gastric corpus and antrum. HO-1 expression was induced only in the CD206-positive macrophages of the gastric corpus (Fig. 3C) and not in the CD206-positive macrophages of the gastric antrum (Fig. 3D).

Effect of CoPP administration on HO-1 and c-Kit expression in STZ-induced diabetic rats

HO-1expression in the stomach was investigated at 8 weeks after STZ injection and CoPP administration (once a week). Immunofluorescence staining demonstrated that CoPP administration significantly increased HO-1 expression both in the gastric corpus and in antrum of the STZ group (Fig. 4A). Western blot analysis also showed that HO-1 expression was not induced by STZ injection (123 ± 35.3% of Normal, $P = 0.31$) but was significantly increased following CoPP administration (436 ± 44.6% of Normal) in the smooth muscle layer of gastric antrum compared to the normal group (Fig. 4B). c-Kit expression was significantly decreased in the smooth muscle layer of the gastric antrum after STZ injection (61.2 ± 19.5% of

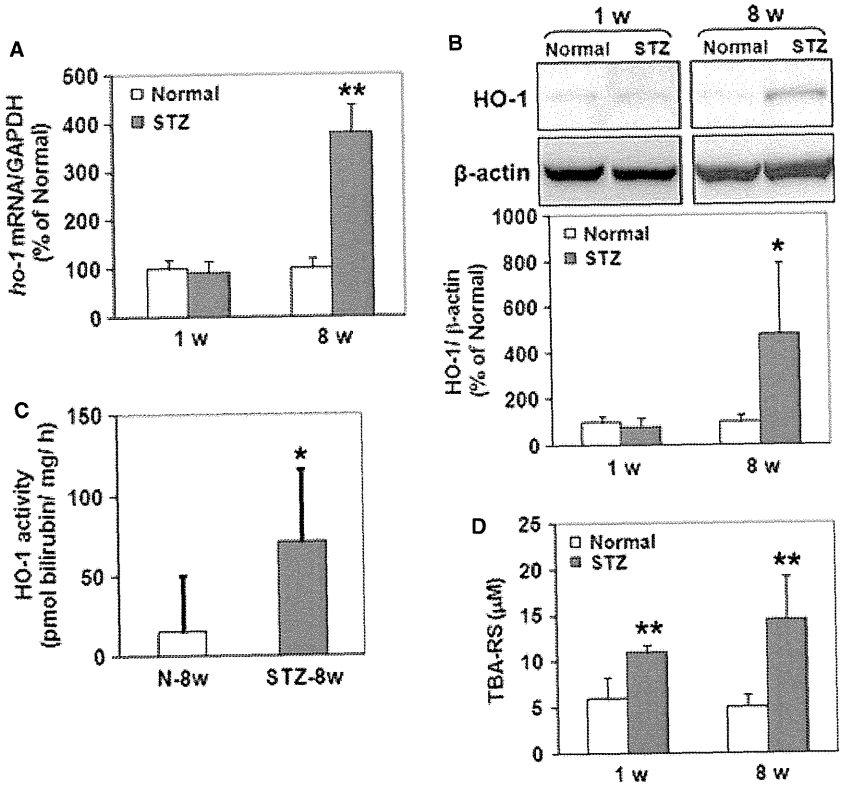

Figure 2 Expression of *ho-1* mRNA in the whole stomach (A) and expression of HO-1 protein in the smooth muscle layer of the whole stomach (B) at 1 and 8 weeks after streptozotocin (STZ) injection. A typical band from each group from the same gel is shown in the upper panel of (B). Bands were quantified and normalized using β-actin as a loading control, and the results are presented as% of Normal in the lower panel. (C) HO-1 activity in the stomach at 8 weeks after STZ injection. (D) Serum TBA-RS levels at 1 week and 8 weeks after STZ injection. Normal-1w (open bar), $n = 6$; STZ-1w (filled bar), $n = 5$; normal-8w (open bar), $n = 6$; STZ-8w (filled bar), $n = 6$. Data are given as means ± SD. $^{*}P < 0.05$, $^{**}P < 0.01$ compared with normal rats.

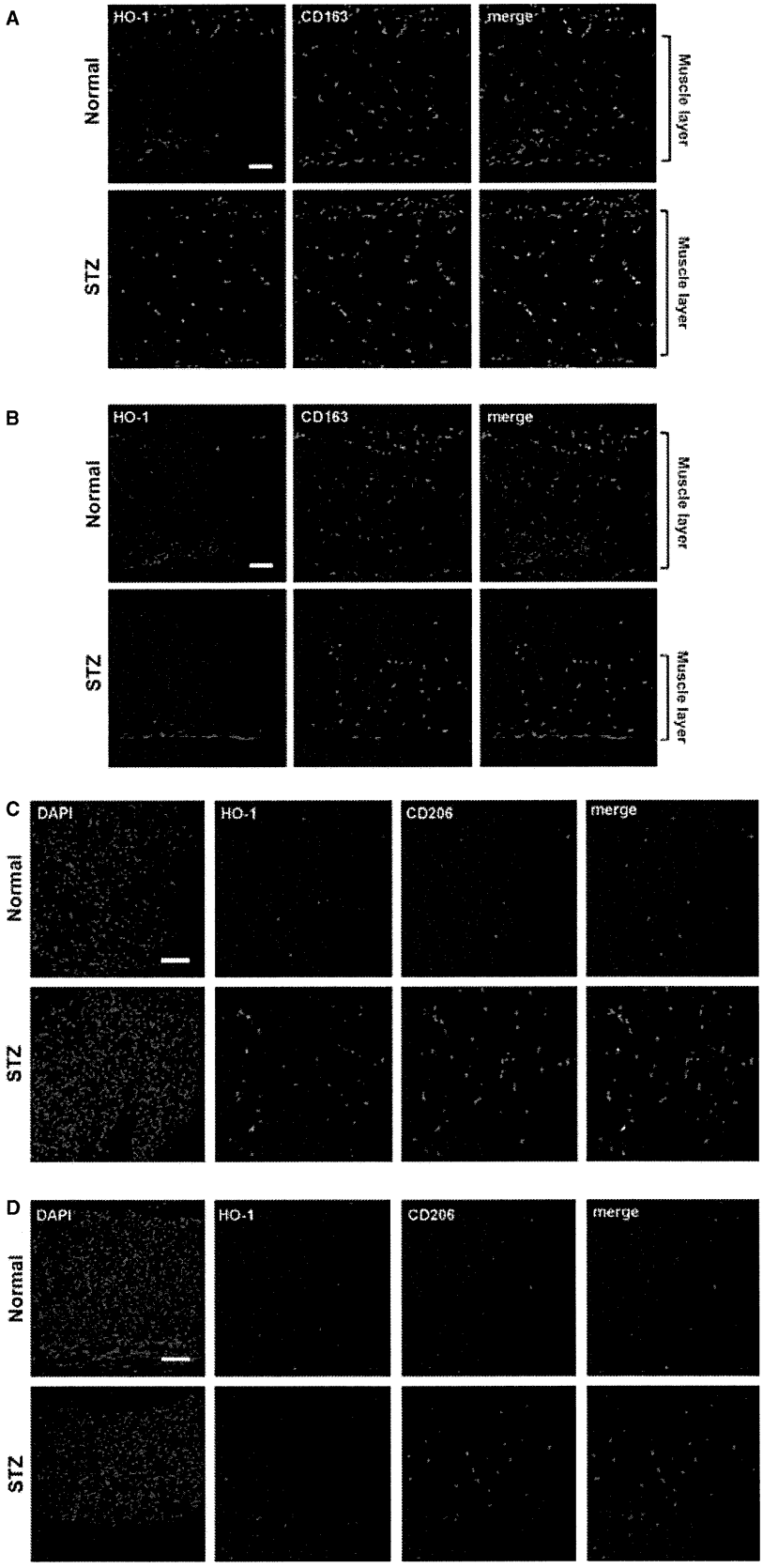

Figure 3 Double immunofluorescence staining (merge, right panel) for HO-1 (left panel, green) and CD163, marker for resident macrophages (middle panel, red), of the smooth muscle layer in the gastric corpus (A) and antrum (B) of normal (upper panel) and streptozotocin (STZ)-induced diabetic rats (lower panel) at 8 weeks after STZ injection. Bar, 100 μm. Double immunofluorescence staining (merge, right panel) for HO-1 (middle panel, green) and CD206, marker for M2 macrophages (middle panel, red), in the smooth muscle layer of gastric corpus (C) and antrum (D) of normal (upper panel) and STZ-induced diabetic rats (lower panel) at 8 weeks after STZ injection. DAPI images are shown in the left panel. Bar, 100 μm.

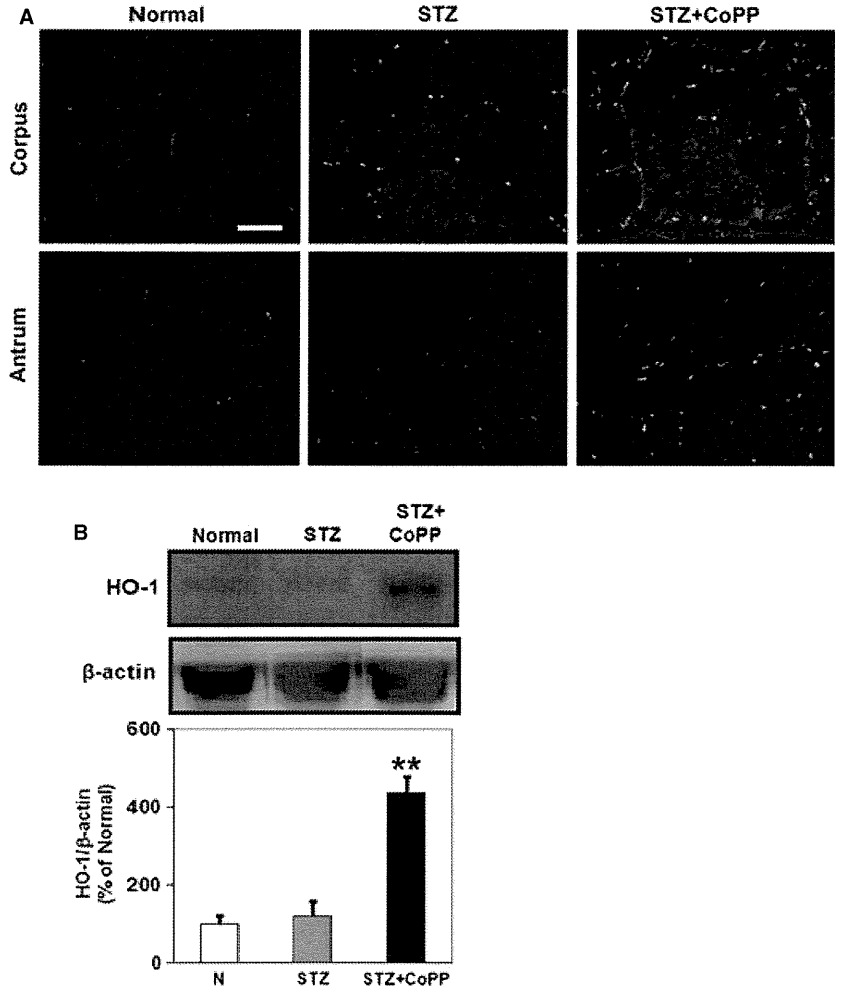

Figure 4 (A) Immunofluorescence staining for HO-1 in the smooth muscle layer of the gastric corpus (upper panel) and antrum (lower panel) of a normal rat (left panel), a streptozotocin (STZ)-treated rat (middle panel), and a STZ + CoPP-treated rat (right panel) at 8 weeks after STZ injection. Bar, 100 μm. (B) Western blot analysis of HO-1 protein expression in the smooth muscle layer of the gastric antrum at 8 weeks after STZ injection. A typical band from each group from the same gel is shown in the upper panel. Bands were quantified and normalized using β-actin as a loading control, and the results are presented as % of Normal in the lower panel. Normal (open bar), $n = 7$; STZ (grey bar), $n = 5$; STZ + CoPP (black bar), $n = 8$. Data are given as means ± SD. $^{**}P < 0.01$ compared with STZ-treated rats.

Normal) and was significantly restored by CoPP administration (82.5 ± 9.02% of Normal) as shown by western blot analysis (Fig. 5A). Immunofluorescence staining revealed that the significantly decreased ICC-IM (68.1 ± 6.10% of Normal) and ICC-SM (49.7 ± 8.73% of Normal) were significantly restored by CoPP administration (89.0 ± 13.4%, 96.4 ± 27.0% of Normal, respectively) in the gastric antrum at 8 weeks after STZ injection (Fig. 5B and C).

DISCUSSION

In this study, we focused on the association between HO-1 induction and the ICC network in an STZ-induced diabetes model. We demonstrated that (i) ICC were significantly decreased only in the gastric antrum at 8 weeks after STZ injection, (ii) HO-1 expression was significantly induced by STZ injection only in the gastric corpus and not in the antrum and (iii) HO-1 induction by CoPP significantly restored the previously decreased ICC in the gastric antrum.

It was reported that the ICC network was disrupted at 8 weeks after STZ injection, particularly in the ICC-IM and ICC-SM in the gastric antrum,[3] which was also observed in this study. The ICC remained unchanged at 1 week after STZ injection; thus, long-term diabetes might have induced the disruption of the ICC network, and not the STZ injection itself.

HO-1 is reported to protect ICC in NOD mice.[2] In the early stage of diabetes, HO-1 was up-regulated in the resident gastric macrophages in all mice. However, in 20% of the diabetic mice, delayed gastric emptying was developed in the late stage of diabetes and c-Kit expression was significantly decreased in the smooth muscle layer of the gastric corpus and antrum. In these mice, the up-regulation of HO-1 was not observed. In the other mice in which delayed gastric emptying and a decrease of c-Kit expression were not observed, HO-1 expression continued to be significantly induced both in the gastric corpus and the antrum.[2] Furthermore, induction of HO-1 by hemin decreased the reactive oxygen species and rapidly restored c-Kit expression in

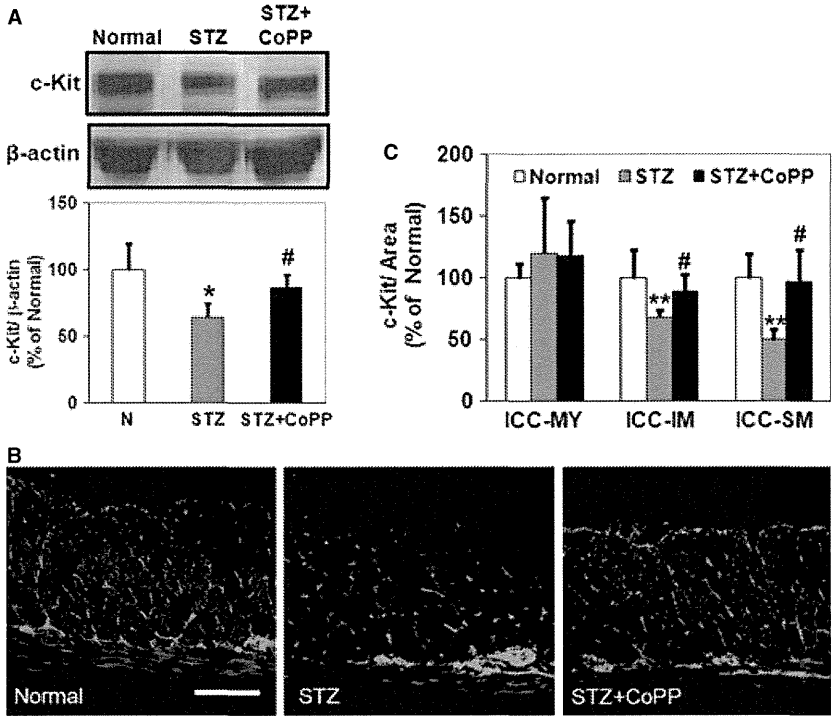

Figure 5 (A) Western blot analysis of c-Kit protein expression in the smooth muscle layer of the gastric antrum at 8 weeks after streptozotocin (STZ) injection. A typical band from each group from the same gel is shown in the upper panel. Bands were quantified and normalized using β-actin as a loading control, and the results are presented as % of Normal in the lower panel. (B) Representative image of Immunofluorescence staining for c-Kit in the smooth muscle layer of the gastric antrum of a normal rat (left panel), a STZ-treated rat (middle panel), and a STZ + CoPP-treated rat (right panel) at 8 weeks after STZ injection. Bar, 100 μm. (C) Areas of ICC-MY, ICC-IM, and ICC-SM in the images of immunofluorescent staining were quantified using image analysis software. Areas of ICC in the gastric antrum are shown. Normal (open bar), $n = 7$; STZ (grey bar), $n = 5$; STZ + CoPP (black bar), $n = 8$. Data are given as means ± SD. $^{*}P < 0.05$, $^{**}P < 0.01$ compared with normal rats, $^{\#}P < 0.05$ compared with STZ-treated rats.

all of the mice. Conversely, inhibition of HO-1 activity by chromium mesoporphyrin caused ICC loss in all mice, suggesting that HO-1 is essential for protecting ICC against oxidative injury.

In the case of STZ-induced diabetic rats, all diabetic rats showed decreased ICC only in the antrum;[3] however, HO-1 induction was not previously elucidated in the STZ diabetic model. Therefore, we investigated the effect of STZ-induced diabetes on HO-1 expression. In this study, the expression of *ho-1* mRNA and HO-1 protein and HO-1 activity were significantly increased at 8 weeks after STZ injection but not at 1 week. The serum TBA-RS levels were significantly increased after 1 week, indicating that exposure to long-term oxidative stress might have induced HO-1 expression. Immunofluorescence staining revealed that HO-1 induction was limited to the gastric corpus suggesting that induction of HO-1 might have protected the ICC from oxidative stress in the gastric corpus but not in the gastric antrum. There appears to be a failure to induce HO-1 expression rather than a loss of up-regulation of HO-1 which developed ICC loss in this model. This finding is different from the previous observation in NOD mice, as up-regulation of HO-1 have always been seen in all mice tested at the 4–5 week time point [2] and loss of up-regulation in some NOD mice in the late stage of diabetes. However, we cannot exclude the possibility that HO-1 was once up-regulated after STZ injection and later it was lost. We only confirmed that HO-1 was not up-regulated at 1 week after STZ injection and up-regulated only in the gastric corpus at 8 week. We administered CoPP, an HO-1 inducer, to up-regulate HO-1 expression in the gastric antrum in the STZ diabetic model. CoPP administration significantly increased HO-1 expression in the antrum and significantly restored the previously decreased c-Kit expression. These results suggest that impaired induction of HO-1 expression in the gastric antrum resulted in the decrease in ICC. The ICC-MY in the gastric antrum were not decreased in the STZ diabetic model which is consistent with the findings of the previous study and those of patients with type 2 diabetes mellitus.[1,3] It is unlikely that only ICC-MY were not exposed to oxidative stress. HO-1 was not induced in STZ diabetic rats also near ICC-MY in the antrum, thus ICC-MY may be protected by factors other than HO-1.

HO-1 expression is induced in the resident macrophages in the gastric smooth muscle layer. In NOD mice and db/db mice, it was reported that alternatively activated macrophages (M2 macrophages) were important for inducing HO-1 expression to protect ICC but not classically activated macrophages (M1 macrophages).[16] In control mice, F4/80-positive resident macrophages were observed, but M2 macrophages were not in the myenteric plexus. In diabetic mice with normal gastric emptying, F4/80-positive resident macrophages were increased and M2 macrophages were also

observed with concomitant HO-1 expression. However, M2 macrophage was not observed in diabetic mice with delayed gastric emptying and a loss of HO-1 induction.

In rats, the monoclonal antibody ED2, which reacts with CD163, is used to detect resident rat macrophages.[17–19] Therefore, we investigated whether HO-1 expression was induced in resident macrophages in the STZ diabetic model. In this study, resident macrophages were observed in the gastric smooth muscle layer of both the normal and STZ diabetic groups on CD163 staining. However, HO-1 expression was up-regulated only in the gastric corpus but not in the resident macrophages of the gastric antrum in STZ rats. Therefore, we investigated whether the gastric corpus and antrum showed different phenotypes in STZ rats. We performed CD206 immunofluorescent staining, which is specific for M2 macrophages, at 8 weeks after STZ injection. In this study, M2 phenotype macrophages were scarcely observed in control rats. In STZ rats, CD206-positive cells were markedly increased in both the gastric corpus and antrum. However, HO-1 expression was up-regulated in the gastric corpus but not in the M2 macrophages of the gastric antrum. These results indicate that the differential induction of HO-1 between the gastric corpus and antrum in the STZ diabetic model is not due to the phenotype of the resident macrophages or the number of macrophages, but probably due to the different properties of the M2 macrophages between the gastric corpus and antrum.

Various transcription factors mediate the induction of HO-1 in response to external and internal stimuli.[20] The transcription factor NF-E2-related factor 2 (Nrf2) is known to induce antioxidant enzymes expression, including HO-1, through antioxidant response.[21] Another transcriptional regulator, Bach1, is a heme binding protein that forms heterodimers with small proteins of the Maf family and represses transcription of the *ho-1* gene by binding to the ARE in the HO-1 promoter.[21] CoPP was reported to up-regulate HO-1 by increasing degradation of the Bach1 protein and decreasing degradation of the Nrf2 protein.[22] Therefore, these transcriptional systems exist in the M2 macrophages of the STZ diabetic model both in the gastric corpus and antrum, as HO-1 expression was induced similarly by CoPP administration in this study. Differential Nrf2 and Bach1 balance between the gastric corpus and antrum or Nrf2-independent pathways (which should be different between the gastric corpus and antrum) may be involved in the different HO-1 induction.[23,24]

In conclusion, induction of HO-1 was limited to the gastric corpus of the STZ-induced diabetic rats at 8 weeks after STZ injection. The up-regulated expression of HO-1 in the corpus might have protected the ICC in the stomach of the STZ group. However, the decreased number of ICC in the antrum was likely due to the impaired up-regulation of HO-1, as it was restored by HO-1 induction.

FUNDING

This study was supported by a Grant-in-Aid for challenging Exploratory Research (24659103, to H.S.), a Grant from the JSPS Bilateral Joint Projects with Belgium (FWO; 11035231-000061, to H.S.), a Grant from the JSPS Bilateral Joint Projects with Korea (NRF; 12032211-000109, to H.S.), a Research Fund of Mitsukoshi Health and Welfare Foundation (to H.S.), a grant of the MEXT-Supported Programme for the Strategic Research Foundation at Private Universities, 2012 (to H.T.), a grant from the Smoking Research Foundation (to H.S.), and the Keio Gijuku Academic Development Funds (to H.S.).

DISCLOSURES

S. Mogami is employed by Tsumura & Co. H. Suzuki had received grant support from Tsumura & Co from 2007 to 2009. H. Tsugawa, S. Fukuhara, T. Hibi have no conflicts of interest to declare.

AUTHOR CONTRIBUTIONS

SM performed the experiments, analysed the data and drafted the manuscript; HS designed the research protocol and reviewed the data and drafted the manuscript; HT, SF analysed and reviewed the data; TH supervised.

REFERENCES

1 Iwasaki H, Kajimura M, Osawa S *et al.* A deficiency of gastric interstitial cells of Cajal accompanied by decreased expression of neuronal nitric oxide synthase and substance P in patients with type 2 diabetes mellitus. *J Gastroenterol* 2006; **41**: 1076–87.

2 Choi KM, Gibbons SJ, Nguyen TV *et al.* Heme oxygenase-1 protects interstitial cells of Cajal from oxidative stress and reverses diabetic gastroparesis. *Gastroenterology* 2008; **135**: 2055–64, 2064, e2051-2052.

3 Wang XY, Huizinga JD, Diamond J, Liu LW. Loss of intramuscular and submuscular interstitial cells of Cajal and associated enteric nerves is related to decreased gastric emptying in streptozotocin-induced diabetes. *Neurogastroenterol Motil* 2009; **21**: 1095, e1092.

4 Huizinga JD, Thuneberg L, Kluppel M, Malysz J, Mikkelsen HB, Bernstein A. W/kit gene required for interstitial cells of Cajal and for intestinal pacemaker activity. *Nature* 1995; **373**: 347–9.

5 Ward SM, Burns AJ, Torihashi S, Sanders KM. Mutation of the proto-oncogene c-kit blocks development of interstitial cells and electrical rhythmicity in murine intestine. *J Physiol* 1994; **480**(Pt 1): 91–7.

6 Suzuki S, Suzuki H, Horiguchi K *et al.* Delayed gastric emptying and disruption of the interstitial cells of Cajal network after gastric ischaemia and reperfusion. *Neurogastroenterol Motil* 2010; **22**: 585–593, e126.

7 Torihashi S, Ward SM, Sanders KM. Development of c-Kit-positive cells and the onset of electrical rhythmicity in murine small intestine. *Gastroenterology* 1997; **112**: 144–55.

8 Ward SM, Harney SC, Bayguinov JR, McLaren GJ, Sanders KM. Development of electrical rhythmicity in the murine gastrointestinal tract is specifically encoded in the tunica muscularis. *J Physiol* 1997; **505**(Pt 1): 241–58.

9 Sanders KM. A case for interstitial cells of Cajal as pacemakers and mediators of neurotransmission in the gastrointestinal tract. *Gastroenterology* 1996; **111**: 492–515.

10 Burns AJ, Lomax AE, Torihashi S, Sanders KM, Ward SM. Interstitial cells of Cajal mediate inhibitory neurotransmission in the stomach. *Proc Natl Acad Sci U S A* 1996; **93**: 12008–13.

11 Ward SM, Beckett EA, Wang X, Baker F, Khoyi M, Sanders KM. Interstitial cells of Cajal mediate cholinergic neurotransmission from enteric motor neurons. *J Neurosci* 2000; **20**: 1393–403.

12 Mitsui R, Komuro T. Distribution and ultrastructure of interstitial cells of Cajal in the gastric antrum of wild-type and Ws/Ws rats. *Anat Embryol (Berl)* 2003; **206**: 453–60.

13 Faussone-Pellegrini MS. Relationships between neurokinin receptor-expressing interstitial cells of Cajal and tachykininergic nerves in the gut. *J Cell Mol Med* 2006; **10**: 20–32.

14 Abraham NG, Asija A, Drummond G, Peterson S. Heme oxygenase -1 gene therapy: recent advances and therapeutic applications. *Curr Gene Ther* 2007; **7**: 89–108.

15 Kashyap PC, Choi KM, Dutta N *et al.* Carbon monoxide reverses diabetic gastroparesis in NOD mice. *Am J Physiol Gastrointest Liver Physiol* 2010; **298**: G1013–9.

16 Choi KM, Kashyap PC, Dutta N *et al.* CD206-positive M2 macrophages that express heme oxygenase-1 protect against diabetic gastroparesis in mice. *Gastroenterology* 2010; **138**: 2399–409, 2409, e2391.

17 Kinoshita K, Horiguchi K, Fujisawa M *et al.* Possible involvement of muscularis resident macrophages in impairment of interstitial cells of Cajal and myenteric nerve systems in rat models of TNBS-induced colitis. *Histochem Cell Biol* 2007; **127**: 41–53.

18 Ohama T, Hori M, Momotani E, Elorza M, Gerthoffer WT, Ozaki H. IL-1beta inhibits intestinal smooth muscle proliferation in an organ culture system: involvement of COX-2 and iNOS induction in muscularis resident macrophages. *Am J Physiol Gastrointest Liver Physiol* 2007; **292**: G1315–22.

19 Chokechanachaisakul U, Kaneko T, Yamanaka Y *et al.* Gene expression analysis of resident macrophages in lipopolysaccharide-stimulated rat molar pulps. *J Endod* 2011; **37**: 1258–63.

20 Ryter SW, Alam J, Choi AM. Heme oxygenase-1/carbon monoxide: from basic science to therapeutic applications. *Physiol Rev* 2006; **86**: 583–650.

21 Loboda A, Jazwa A, Grochot-Przeczek A *et al.* Heme oxygenase-1 and the vascular bed: from molecular mechanisms to therapeutic opportunities. *Antioxid Redox Signal* 2008; **10**: 1767–812.

22 Shan Y, Lambrecht RW, Donohue SE, Bonkovsky HL. Role of Bach1 and Nrf2 in up-regulation of the heme oxygenase-1 gene by cobalt protoporphyrin. *FASEB J* 2006; **20**: 2651–3.

23 Piao MS, Park JJ, Choi JY *et al.* Nrf2-dependent and Nrf2-independent induction of phase 2 detoxifying and antioxidant enzymes during keratinocyte differentiation. *Arch Dermatol Res* 2012; **304**: 387–95.

24 Reisman SA, Aleksunes LM, Klaassen CD. Oleanolic acid activates Nrf2 and protects from acetaminophen hepatotoxicity via Nrf2-dependent and Nrf2-independent processes. *Biochem Pharmacol* 2009; **77**: 1273–82.

United European Gastroenterology Journal
http://ueg.sagepub.com/

Validation of the GerdQ questionnaire for the management of gastro-oesophageal reflux disease in Japan

Hidekazu Suzuki, Juntaro Matsuzaki, Sawako Okada, Kenro Hirata, Seiichiro Fukuhara and Toshifumi Hibi
United European Gastroenterology Journal published online 10 April 2013
DOI: 10.1177/2050640613485238

The online version of this article can be found at:
http://ueg.sagepub.com/content/early/2013/04/02/2050640613485238

Published by:
SAGE
http://www.sagepublications.com

On behalf of:
United European Gastroenterology

UNITED EUROPEAN GASTROENTEROLOGY ueg journal

Original Article

United European Gastroenterology Journal
0(0) 1–9

DOI: 10.1177/2050640613485238
ueg.sagepub.com
SAGE

Validation of the GerdQ questionnaire for the management of gastro-oesophageal reflux disease in Japan

Hidekazu Suzuki, Juntaro Matsuzaki, Sawako Okada, Kenro Hirata, Seiichiro Fukuhara and Toshifumi Hibi

Abstract

Background: The GerdQ scoring system may be a useful tool for managing gastro-oesophageal reflux disease. However, GerdQ has not been fully validated in Asian countries.

Objective: To validate the Japanese version of GerdQ and to compare this version to the Carlsson-Dent questionnaire (CDQ) in both general and hospital-based populations.

Methods: The questionnaires, including the Japanese versions of GerdQ and CDQ, and questions designed to collect demographic information, were sent to a general population via the web, and to a hospital-based population via conventional mail. The optimal cutoff GerdQ score and the differences in the characteristics between GerdQ and CDQ were assessed.

Results: The answers from 863 web-responders and 303 conventional-mail responders were analysed. When a GerdQ cutoff score was set at 8, GerdQ significantly predicted the presence of reflux oesophagitis. Although the GerdQ scores were correlated with the CDQ scores, the concordance rates were poor. Multivariate analysis results indicated that, the additional use of over-the-counter medications was associated with GerdQ score ≥ 8, but not with CDQ score ≥ 6.

Conclusions: The GerdQ cutoff score of 8 was appropriate for the Japanese population. Compared with CDQ, GerdQ was more useful for evaluating treatment efficacy and detecting patients' unmet medical needs.

Keywords

Cutoff, GerdQ, GERD, questionnaire, unmet medical need

Received: 22 January 2013; accepted: 12 March 2013

Introduction

The prevalence of gastro-oesophageal reflux disease (GERD) is dramatically increasing in both Western and Asian countries, including Japan.[1] To diagnose GERD objectively, invasive examinations such as oesophagogastroduodenoscopy and pH monitoring can be employed. However, these methods are inconvenient to patients and have limited availability for primary care physicians. Therefore, the current guidelines recommend a symptom-based approach for diagnosis and treatment, especially in the primary care of young patients, who have a short disease history and no alarm symptoms.[2] Primary care physicians experience the challenge of accurately diagnosing and effectively managing GERD with drugs that meet patients' satisfaction.

GerdQ is a self-administered 6-item questionnaire that was recently developed as a tool to improve and standardize symptom-based diagnosis and evaluation of treatment response in patients with GERD.[3] Norwegian researchers assessed the diagnostic validity of GerdQ, and they concluded that GerdQ is a useful, complementary tool for diagnosing GERD in primary care.[4] They also reported that a symptom-based approach using GerdQ reduced healthcare costs without a loss in efficacy.[5]

In the development of GerdQ, GERD was diagnosed if patients fulfilled at least one of the following criteria: (i) oesophageal pH < 4 for $>5.5\%$ of a 24-h period, (ii) Los Angeles (LA) grade A–D oesophagitis at endoscopy, (iii) indeterminate 24-h oesophageal pH

Keio University School of Medicine, Tokyo, Japan

Corresponding author:
Hidekazu Suzuki, 35 Shinanomachi, Shinjuku-ku, Tokyo 160-8582, Japan.
Email: hsuzuki@a6.keio.jp

in combination with a positive response to 14 days' esomeprazole treatment, and (iv) positive (>95) symptom association probability (SAP).[3] This suggests that the GerdQ scores might be well correlated with the severity of acid reflux. In the East Asia and Pacific regions, lower gastric acid secretion is generally observed, and the prevalence of reflux oesophagitis is comparatively low.[6–8] Therefore, the validation of GerdQ in Asian countries is important.

In the present study, we evaluated the usefulness of the Japanese version of GerdQ in two different Japanese populations: general and hospital-based populations. Among the hospital-based population, the association between the GerdQ score and the presence of reflux oesophagitis was assessed. In addition, to clarify the characteristics of GerdQ, the differences in the characteristics between the GerdQ and the Carlsson-Dent questionnaire (CDQ), which is a traditional questionnaire used for diagnosing GERD,[9–11] were investigated.

Materials and methods

Study population

The present study was approved by the ethics committee of the Keio University School of Medicine (2010–319, 5 April 2011). The questionnaires, which comprised the Japanese versions of GerdQ and CDQ, demographic information (age, gender, smoking habits, alcohol consumption, height, weight, and past medical history), and treatment history for upper gastrointestinal symptoms involving prescription or over-the-counter (OTC) medicine use, were sent to both a web-based and conventional mail-surveyed population. Participants for the web-based survey were randomly selected from subjects who had registered with a web-survey company and who had a present or past history of heartburn and/or regurgitation. They provided informed consent by checking a web box. On the other hand, patients who underwent oesophagogastroduodenoscopy at the Keio University Hospital between December 2010 and May 2011 were enrolled in the mail survey. The mails were sent in June 2011. Participants with malignant diseases, peptic ulcers, a history of gastric surgery, or systematic diseases affecting the upper gastrointestinal tract were excluded. Participants with heartburn and/or regurgitation more frequently than once a week were defined as having GERD.[12] The presence of erosive oesophagitis or positive proton pump inhibitor (PPI) response has not been taken into account for the diagnosis of GERD in the present study.

Individuals were categorized as 'non-smokers', 'ex-smokers', '1–15 cigarettes/day', and '> 15 cigarettes/day', according to the number of cigarettes consumed per day. With regard to alcohol consumption, individuals were categorized as 'abstainers', 'social drinkers', 'stopped drinking', '1–2 days/week', '3–4 days/week', and '5–7 days/week', according to the number of days alcohol was consumed per week. Body mass index (BMI, weight/height^2) was calculated. Participants were diagnosed with metabolic syndrome if they were overweight (BMI $\geq 25\,kg/m^2$) or they had hypertension, diabetes mellitus, or dyslipidaemia, according to their responses on the questionnaire.[13] For participants who responded via the mail survey, the severity of reflux oesophagitis was investigated using medical records.

Statistical analysis

Comparisons of two categorical variables such as gender and the presence/absence of diabetes, hypertension, dyslipidaemia, fatty liver, or the use of each medication were analysed using Fisher's Exact test. Other categorical variables such as smoking and alcohol consumption were analysed using Pearson's χ^2 test. Continuous variables such as age and BMI were analysed using Student's t-test. The cutoff value for the CDQ was set at 6, whereas the cutoff value of GerdQ was set at 8, in accordance with previous reports.[3,9] The GerdQ cutoff value for predicting the presence of reflux oesophagitis was validated among the mail-surveyed population by using receiver operating characteristic (ROC) analysis. Subsequently, the correlations between the CDQ and GerdQ scores were analysed using Pearson's correlation analysis, and the concordance rates (kappa coefficient) were calculated between CDQ score ≥ 6 and GerdQ score ≥ 8. Finally, the associations of CDQ score ≥ 6 or GerdQ score ≥ 8 with demographic factors were analysed using univariate and multivariate logistic regression models. The multivariate logistic regression model was adjusted for age, gender, the presence of metabolic syndrome, and the use of both prescription and OTC medications. All statistical analyses were conducted using SPSS Statistics version 18.0 for Windows software (SPSS Japan, Tokyo, Japan). Two-sided p-values were considered statistically significant at a level of 0.05.

Results

Characteristics of participants

In the web survey, a total of 1630 participants were sent questionnaires, among which 1024 complete responses were received (Figure 1a). After excluding participants with malignant diseases ($n = 30$) and those with peptic ulcers ($n = 131$), the responses of the remaining 863 participants were used in the analysis. Among them, 362